crystals

MDPI

Article

Electromechanically Rotatable Cross-Shaped Mid-IR Metamaterial

Jitong Zhong and Yu-Sheng Lin *

State Key Laboratory of Optoelectronic Materials and Technologies, School of Electronics and Information Technology, Sun Yat-Sen University, Guangzhou 510275, China; zhongjt5@mail2.sysu.edu.cn

* Correspondence: linyoush@mail.sysu.edu.cn

Received: 15 May 2020; Accepted: 27 May 2020; Published: 28 May 2020

Abstract: We present an electromechanically rotatable infrared (IR) cross-shaped metamaterial (CSM) in the mid-IR wavelength range. The CSM configuration is composed of double gold layers with cross-shaped nanostructures. To investigate the fano-resonance within CSM nanostructures, the aspect ratios and length ratios of CSM are compared and discussed. The electromagnetic responses exhibit the characteristics of large tuning range, tunable broad and narrow bandwidths. By properly tailoring the aspect ratio of CSM, the resonance can be tuned with bidirectional tuning in the range of 650 nm. CSM with different length ratios exhibit narrowband resonances around the wavelength of 4.6 μm and broadband resonances in the wavelength range of 5.0 μm to 6.5 μm. These characteristics of CSM with different aspect ratios and length ratios could be potentially used in IR narrowband and broadband filter. To further increase the flexibility of proposed electromechanically rotatable CSM, an actively tunable narrowband and broadband filter in the mid-IR wavelength range is performed. This study provides a unique approach to realizing an IR filter, with high flexibility.

Keywords: electromechanically; rotatability; metamaterials; multi-functionalities; IR filter

1. Introduction

Metamaterials are artificial materials that make humans capable of controlling the electromagnetic wave by properly tailoring. They have been widely reported and demonstrated in many fields, such as high-sensitive sensors, cloaking devices, security screening, perfect absorbers, tunable filters, light emitters, imaging devices, and non-destructive testing [1–16]. Among these applications, the tunable metamaterial filter is one of most important optoelectronic devices to filter a certain resonant frequency for widespread applications [17–21].

To meet the requirements of certain functions in the real-world applications, the active tunability is attractive to make metamaterials possess high flexibility and applicability. Therefore, the suitable tuning methods of metamaterials are required to improve the metamaterial performances and tunabilities of optical characteristics, which has long been a research topic of interest for scientists. There have been reported many literatures to demonstrate tunable metamaterials by using thermal annealing, ferroelectric materials, semiconductor materials or diodes, laser pumping, liquid crystal, electrostatic force, and microelectromechanical systems (MEMS) technology [17–23]. Among these tuning approaches, MEMS technology is an alternative method to directly change the geometrical structures of metamaterials. It involves semiconductor, electronic engineering, mechanical engineering, medicine, physics, information engineering and other disciplines and technologies [24–28]. It is an independent intelligent system. There have been many MEMS-based tunable metamaterials reported, including MEMS-based resonant cloaking metamaterial [29], active phase transition metamaterial [30], tunable ultrathin metamaterial [31], CMOS-MEMS broadband metamaterial [32], electromagnetically induced metamaterial [33], MEMS-modulated metamaterial [34], and so on. However, these approaches cannot

be controlled, and manipulated the unit cell by unit cell. Therefore, these proposed MEMS-based approaches are limited in certain applications and have less tuning range, which will confine their flexibility and applicability in real-world applications.

To overcome the above-mentioned confinements, we propose a tunable cross-shaped metamaterial (CSM) using MEMS technology. CSM is composed of top and bottom tailored Au layers, which can be realized by using MEMS technology to derive an electrothermal actuation force to perform the cross-shaped nanostructures rotated at an angle and then tune the resonant frequency. It can be electromechanically rotated CSM unit cell individually. By changing these geometrical configurations, CSM shows different electromagnetic characteristics and flexible tunability. The corresponding fano-resonances within CSM nanostructures are investigated to figure out the suitable design.

2. Materials and Methods

Figure 1a shows the schematic drawing of MEMS-based CSM and the corresponding CSM unit cell. It is composed of double tailored Au layers with a gap between them. The top Au layer is connected to a poly-Si electro-thermal actuator, which can be rotated by driving different voltages to exhibit high flexibility. The geometrical parameters are metallic lengths along x- and y-axis directions, which are denoted as L_1 and L_2, respectively. The metallic width (W) of CSM is varied simultaneously when discussing the electromagnetic characteristics in this study. The metallic thicknesses of two Au layers are kept as constant as 200 nm. The gap is also kept as constant as 100 nm. The reconfiguration of CSM is proposed to compare and discuss different aspect ratios ($t = W/L$), length ratios ($r = L_1/L_2$), and rotation angles of the top metamaterial layer. The fabrication process of MEMS-based CSM device is illustrated in Figure 1b. First, an Au thin-film with 200 nm in thickness was deposited by using lift-off process, as shown in Figure 1b-i. Second, SiO_2 and poly-Si thin-films with 500 nm and 40 nm in thicknesses, respectively, were deposited by using the plasma enhanced chemical vapor deposition (PECVD) process, as shown in Figure 1b-ii. Third, poly-Si thin-film was patterned by using the reactive ion etching (RIE) process, as shown in Figure 1b-iii. Fourth, an Au thin-film was deposited by using the lift-off process, as shown in Figure 1b-iv. Finally, the nanostructures were released by using vapor HF, as shown in Figure 1b-v. In the future, we will design and demonstrate CSM device by using MEMS technology and following up this fabrication process. Such CSM device possesses flexibility and applicability which could be used in widespread applications with active tunability, such as switch, filter, absorber, sensor, and so on.

The optical properties of the proposed CSM device are simulated through Lumerical Solution's finite difference time domain (FDTD)-based simulations (LUMERICAL version: 8.12.631). The propagation direction of incident light is set to be perpendicular to the x-y plane in the numerical simulations. Periodic boundary conditions are also adopted in the x- and y-axis directions, and perfectly matched layer (PML) boundaries conditions are assumed in the z-axis direction. The reflection (R) and transmission (T) of lights are calculated by two monitors set on both sides of the device. In these configurations, Si material serves as the substrate with the tailored Au layer atop. The permittivity values of Au and Si materials in the mid-IR wavelength range are calculated according to the Drude-Lorentz model [35,36].

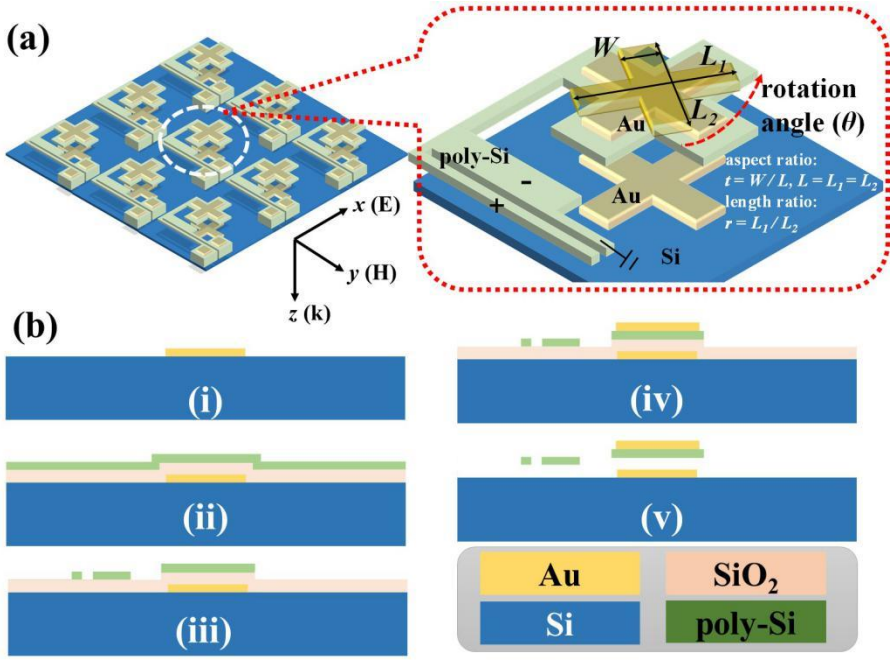

Figure 1. (**a**) Schematics drawing of electromechanically rotatable cross-shaped metamaterial (CSM) array and the corresponding denotations of geometrical parameters. (**b**) Fabrication process flow of proposed CSM device. (**b-i**) The deposition of Au thin-film with 200 nm in thickness by using lift-off process. (**b-ii**) SiO_2 and poly-Si thin-films with 500 nm and 40 nm in thicknesses, respectively, were deposited by using plasma enhanced chemical vapor deposition (PECVD) process. (**b-iii**) Poly-Si thin-film was patterned by using reactive ion etching (RIE) process. (**b-iv**) The deposition of Au thin-film with 200 nm in thickness by using lift-off process. (**b-v**) The nanostructures were released by using vapor HF.

3. Results and Discussions

The transmission and reflection spectra of CSM with different t (W/L) values in mid-IR wavelength range under the condition of $L = L_1 = L_2 = 2000$ nm are shown in Figure 2a,b, respectively. When t value is 0.2, i.e., W/L = 400 nm/2000 nm, the resonances of transmission and reflection spectra are at the wavelength of 5.38 μm. By increasing t value from 0.2 to 1.0 (from W/L = 400 nm/2000 nm to W/L = 2000 nm/2000 nm) in 0.2 steps, the resonances are blue-shifted 230 nm from t = 0.2 to t = 0.4 (from W/L = 400 nm/2000 nm to W/L = 800 nm/2000 nm), and then red-shifted 650 nm from t = 0.4 to t = 1.0 (from W/L = 800 nm/2000 nm to W/L = 2000 nm/2000 nm). These results clearly show that CSM exhibits a bidirectional characteristic by changing t value under the condition of $L = L_1 = L_2 = 2000$ nm. The transmission spectra of CSM with different r (L_1/L_2) values under the conditions of W = 200 nm, 400 nm, 800 nm and 1200 nm, by keeping the $L_1 = L_2 = 2000$ nm, are shown in Figure 3. In Figure 3a, the resonant peak is blue-shifted 50 nm from the wavelength of 4.70 μm (r = 0.2) to 4.65 μm (r = 1.0) and the resonant dip is blue-shifted 30 nm from the wavelength of 5.58 μm (r = 0.2) to 5.55 μm (r = 1.0). By increasing the metallic width to 400 nm (W = 400 nm), the resonant peak is blue-shifted 100 nm from the wavelength of 4.66 μm (r = 0.2) to 4.56 μm (r = 1.0), and the resonant dip is blue-shifted 140 nm from the wavelength of 5.52 μm (r = 0.2) to 5.38 μm (r = 1.0), as shown in Figure 3b. When W = 800 nm, the first resonance is red-shifted 330 nm from the wavelength of 4.82 μm (r = 0.4) to 5.15 μm (r = 1.0), and the second resonance is red-shifted 340 nm from the wavelength of 6.08 μm (r = 0.4) to 5.38 μm (r = 0.6), as shown in Figure 3c. In the case of W = 1200, the full width at half maximum (FWHM) of resonance can be tuned from 180 nm to 520 nm, by changing r = 0.6 to r = 1.0 in 0.1 steps, as shown in Figure 3d.

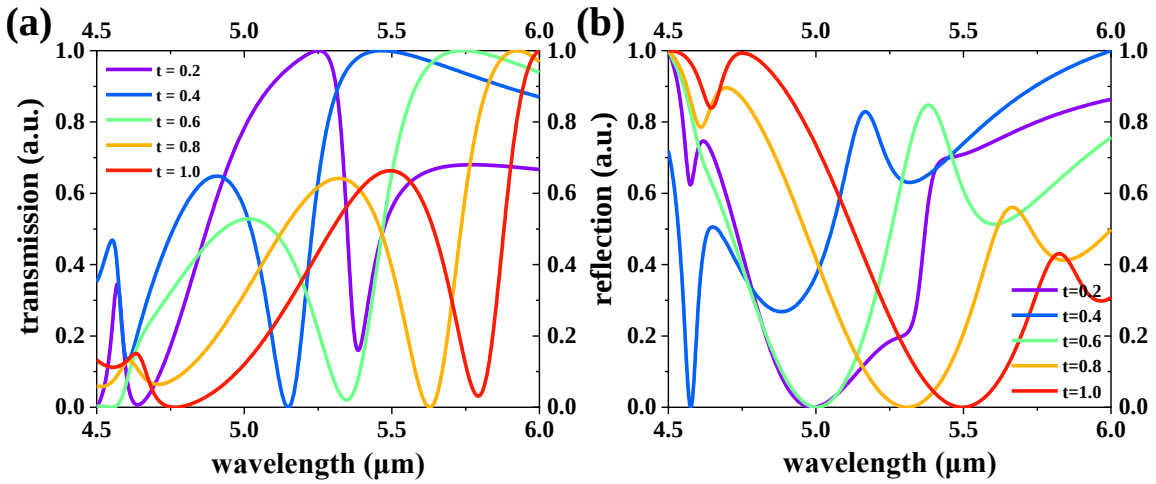

Figure 2. (**a**) Transmission and (**b**) reflection spectra of CSM with different t values under the condition of $L = L_1 = L_2$.

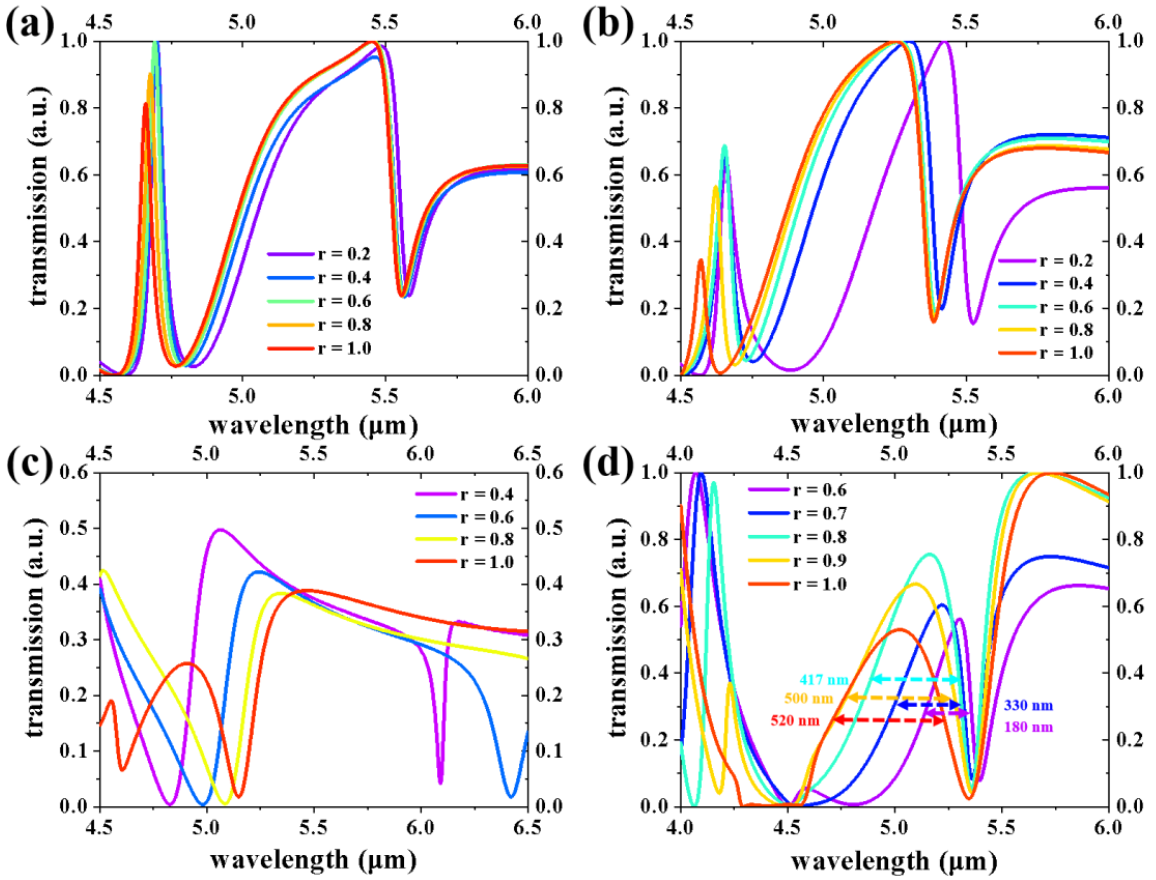

Figure 3. Transmission spectra of CSM with different r values under the conditions of (**a**) W = 200 nm, (**b**) W = 400 nm, (**c**) W = 800 nm, and (**d**) W = 1200 nm, respectively.

To further investigate the tunability of an electromechanically rotatable CSM device, it is designed to rotate an angle between double tailored Au layers by using MEMS-based electrothermal actuator. Figure 4a shows the layout of a CSM unit cell. The lengths of hot arm (L_h), cold arm (L_c), flexure (L_f) and connecting rod (L_3) are 4800 nm, 4000 nm, 800 nm and 1400 nm, respectively. The widths of hot arm, flexure, and connecting rod are 50 nm, while the width of cold arm (w_c) is 500 nm. The total thickness (h) of electrothermal actuator is 40 nm. Herein, the reconfiguration of electromechanically

rotatable CSM is proposed, to compare and discuss different rotation angles of top metamaterial layer, by driving different voltages on electrothermal actuator. The displacement is generated through the asymmetric heating of hot and cold arms. By driving a voltage on CSM device, the higher current density in narrower hot arm will expand more than that of the wider cold arm. The arms are jointed at the free end, where the driving force of actuator moves the CSM laterally in an arcing motion towards the cold arm side [37]. According to the equation of the U-shaped electrothermal actuator, the deflection in the free end of actuator is linear to the driving voltage [37]. The relationship of driving voltages and displacements of electromechanically rotatable CSM device are summarized in Figure 4b. The maximum driving voltage is 20 volts, to actuate the CSM unit cell rotated to 45°. The surface thermal flows of electrothermal actuator at the driving voltages of 12 volts, 14 volts, 16 volts, and 20 volts are simulated using COMSOL software, which are plotted in Figure 5a–d, respectively. Here, we choose the condition of CSM with W = 800 nm, as an example to demonstrate that the electromechanically rotatable CSM can be realized by using a MEMS-based electrothermal actuator. Figure 6a,b show the transmission and reflection spectra of electromechanically rotatable CSM device with different rotation angles, respectively. By changing the rotation angle as 0°, 15°, 30°, and 45°, the resonances of transmission spectra can be tuned to the FWHM values of the CSM device, i.e., spectrum bandwidth as 300 nm, 650 nm, 1040 nm, and 1200 nm, respectively, as shown in Figure 6a, while the narrowband resonance of reflection spectra is blue-shifted 200 nm from the wavelength of 4.37 μm to 4.17 μm, as shown in Figure 6b. It is clearly observed that the proposed electromechanically rotatable CSM device exhibits the tunable abilities of broad and narrow bandwidth for the transmission and reflection spectra, respectively. Such tuning approach provides a suitable design for a tunable mid-IR filter application with high flexibility.

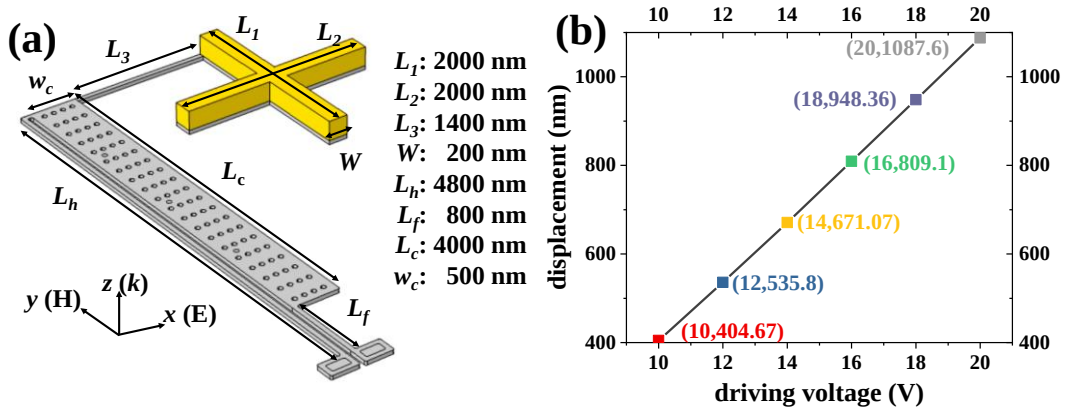

Figure 4. (**a**) Schematic drawing and geometrical dimensions of CSM unit cell. (**b**) The relationship of driving voltages and displacements of electromechanically rotatable CSM.

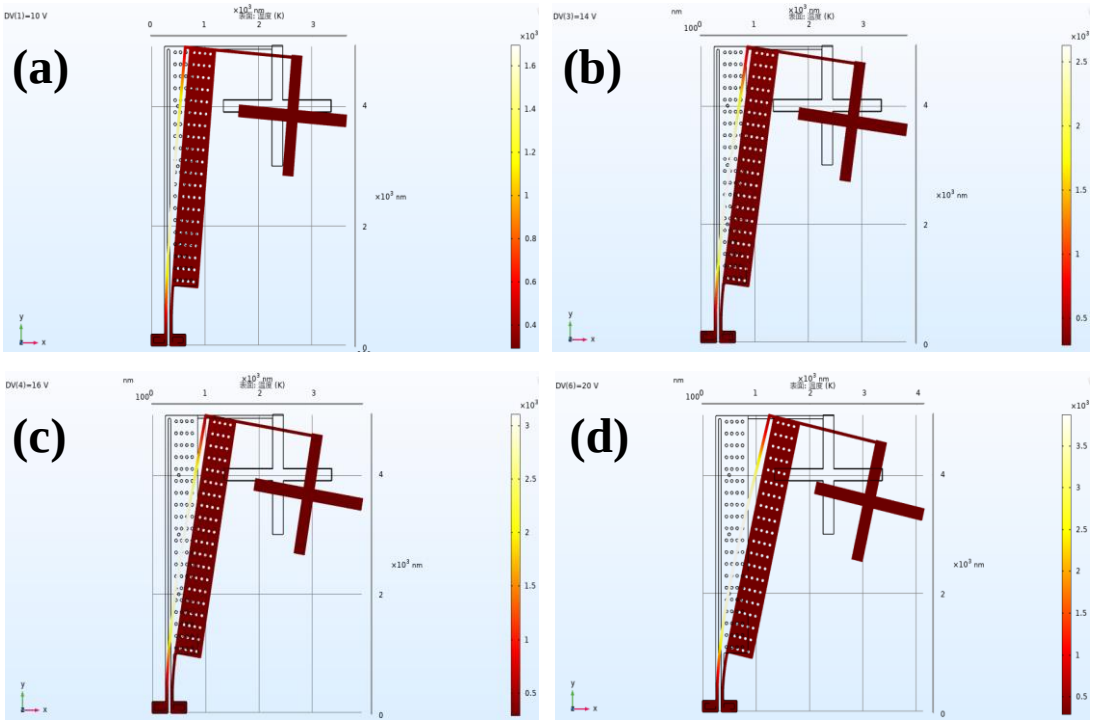

Figure 5. Simulated surface thermal flows of electrothermal actuator at the driving voltages of (**a**) 12 volts, (**b**) 14 volts, (**c**) 16 volts, and (**d**) 20 volts, respectively.

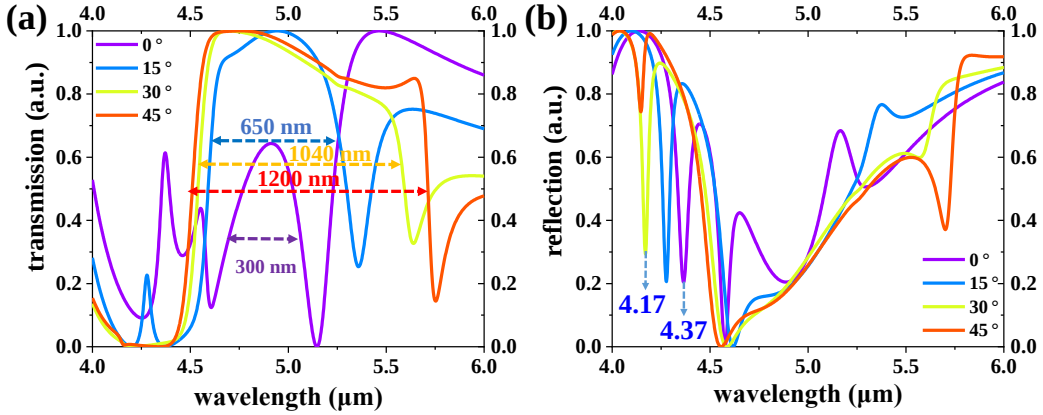

Figure 6. (**a**) Transmission and (**b**) reflection spectra of electromechanically rotatable CSM with different rotation angles under the conditions of W = 800 nm.

4. Conclusions

In conclusion, a reshaping MEMS-based electromechanically rotatable CSM is presented, which is composed of double Au metamaterial layers. By tailoring the geometrical parameters of CSM, the corresponding electromagnetic behavior exhibits tunable bandwidth, large tuning range of resonance, and tunable narrowband resonance characteristics. The variation of t value shows that the resonance could be modified with red-shift of 400 nm and blue-shift of 650 nm to form the bidirectional tuning. Meanwhile, the variation of r value shows that the transmission bandwidths could be modified to be narrow around the wavelength of 4.6 μm and broad in the wavelength range of 5.0 μm to 6.5 μm. These characterizations of CSM with different t and r values could be potentially used in high-efficiency mid-IR narrowband and broadband filter. Furthermore, we propose an active tuning mechanism using a poly-Si MEMS-based electrothermal actuator to increase the flexibility of CSM. This approach exhibits that the bandwidth of CSM could be tuned by rotating the top cross-shaped metamaterial.

By rotating at an angle from 0° to 45° in 15° steps, the electromagnetic bandwidth can be tuned from 300 nm to 1200 nm. It is enhanced 4-fold. These results open an avenue for filter, absorber, detector, sensor, and switch applications with high-flexibility in mid-IR wavelength range.

Author Contributions: Conceptualization, J.Z. and Y.-S. Lin; methodology, J.Z. and Y.-S.L.; formal analysis, J.Z.; investigation, J.Z.; data curation, J.Z.; writing—original draft preparation, J.Z.; writing—review and editing, Y.-S.L.; visualization, Y.-S.L.; supervision, Y.-S.L.; funding acquisition, Y.-S.L. All authors have read and agreed to the published version of the manuscript.

Funding: This research was funded by National Key Research and Development Program of China (2019YFA0705000).

Acknowledgments: The authors acknowledge the State Key Laboratory of Optoelectronic Materials and Technologies of Sun Yat-Sen University, for the use of experimental equipment.

Conflicts of Interest: The authors declare no conflict of interest.

References

1. Kabashin, A.V.; Evans, P.; Pastkovsky, S.; Hendren, W.; Wurtz, G.A.; Atkinson, R.; Pollard, R.; Podolskiy, V.A.; Zayats, A.V. Plasmonic nanorod metamaterials for biosensing. *Nat. Mater.* **2009**, *8*, 867–871. [CrossRef] [PubMed]
2. Sreekanth, K.V.; Alapan, Y.; ElKabbash, M.; Ilker, E.; Hinczewski, M.; Gurkan, U.A.; De Luca, A.; Strangi, G. Extreme sensitivity biosensing platform based on hyperbolic metamaterials. *Nat. Mater.* **2016**, *15*, 621–627. [CrossRef] [PubMed]
3. Garoli, D.; Calandrini, E.; Giovannini, G.; Hubarevich, A.; Caligiuri, V.; De Angelis, F.; Hubarevich, A. Nanoporous gold metamaterials for high sensitivity plasmonic sensing. *Nanoscale Horiz.* **2019**, *4*, 1153–1157. [CrossRef]
4. Lin, Y.-S.; Dai, J.; Zeng, Z.; Yang, B.-R. Metasurface Color Filters Using Aluminum and Lithium Niobate Configurations. *Nanoscale Res. Lett.* **2020**, *15*, 77. [CrossRef] [PubMed]
5. Dai, J.; Xu, R.; Lin, Y.-S.; Chen, C.H. Tunable electromagnetic characteristics of suspended nanodisk metasurface. *Opt. Laser Technol.* **2020**, *128*, 106214. [CrossRef]
6. Lochbaum, A.; Fedoryshyn, Y.; Dorodnyy, A.; Koch, U.; Hafner, C.; Leuthold, J. On-Chip Narrowband Thermal Emitter for Mid-IR Optical Gas Sensing. *ACS Photonics* **2017**, *4*, 1371–1380. [CrossRef]
7. Liu, N.; Mesch, M.; Weiss, T.; Hentschel, M.; Giessen, H. Infrared Perfect Absorber and Its Application as Plasmonic Sensor. *Nano Lett.* **2010**, *10*, 2342–2348. [CrossRef] [PubMed]
8. Mo, Y.; Zhong, J.; Lin, Y.-S. Tunable chevron-shaped infrared metamaterial. *Mater. Lett.* **2020**, *263*, 127291. [CrossRef]
9. Hwang, I.; Yu, J.; Lee, J.; Choi, J.-H.; Choi, D.-G.; Jeon, S.; Lee, J.; Jung, J.-Y. Plasmon-Enhanced Infrared Spectroscopy Based on Metamaterial Absorbers with Dielectric Nanopedestals. *ACS Photonics* **2018**, *5*, 3492–3498. [CrossRef]
10. Liu, P.; Liang, Z.; Lin, Z.; Xu, Z.; Xu, R.; Yao, D.; Lin, Y.-S. Actively tunable terahertz chain-link metamaterial with bidirectional polarization-dependent characteristic. *Sci. Rep.* **2019**, *9*, 9917. [CrossRef]
11. Luo, J.; Lin, Y.-S. High-efficiency of infrared absorption by using composited metamaterial nanotubes. *Appl. Phys. Lett.* **2019**, *114*, 051601. [CrossRef]
12. Lin, Y.-S.; Liao, S.; Liu, X.; Tong, Y.; Xu, Z.; Xu, R.; Yao, D.; Yu, Y. Tunable terahertz metamaterial by using three-dimensional double split-ring resonators. *Opt. Laser Technol.* **2019**, *112*, 215–221. [CrossRef]
13. Dao, T.D.; Ishii, S.; Yokoyama, T.; Sawada, T.; Sugavaneshwar, R.P.; Chen, K.; Wada, Y.; Nabatame, T.; Nagao, T. Hole Array Perfect Absorbers for Spectrally Selective Midwavelength Infrared Pyroelectric Detectors. *ACS Photonics* **2016**, *3*, 1271–1278. [CrossRef]
14. Lin, Y.-S.; Yan, K.; Yao, D.; Yu, Y. Investigation of electromagnetic response of terahertz metamaterial by using split-disk resonator. *Opt. Laser Technol.* **2019**, *111*, 509–514. [CrossRef]
15. Lin, Y.-S. Complementary Infrared Metamaterials for Volatile Organic Solutions Sensing. *Mater. Lett.* **2017**, *195*, 55–57. [CrossRef]
16. Lin, Y.-S.; Chen, W. Perfect meta-absorber by using pod-like nanostructures with ultra-broadband, omnidirectional, and polarization-independent characteristics. *Sci. Rep.* **2018**, *8*, 7150. [CrossRef]

17. Lin, Y.-S.; Chen, W. A large-area, wide-incident-angle, and polarization-independent plasmonic color filter for glucose sensing. *Opt. Mater.* **2018**, *75*, 739–743. [CrossRef]
18. Cheng, S.; Xu, Z.; Yao, D.; Zhang, X.; Zhang, Z.; Lin, Y.-S. Electromagnetically induced transparency in terahertz complementary spiral-shape metamaterials. *OSA Contin.* **2019**, *2*, 2137–2144. [CrossRef]
19. Huang, W.; Xu, R.; Lin, Y.-S.; Chen, C.-H. Three-dimensional pyramid metamaterial with tunable broad absorption bandwidth. *AIP Adv.* **2020**, *10*, 035125. [CrossRef]
20. Hu, X.; Zheng, D.; Lin, Y.-S. Actively tunable terahertz metamaterial with single-band and dual-band switching characteristic. *Appl. Phys. A* **2020**, *126*, 110. [CrossRef]
21. Lin, Z.; Xu, Z.; Liu, P.; Liang, Z.; Lin, Y.-S. Polarization-sensitive terahertz resonator using asymmetrical F-shaped metamaterial. *Opt. Laser Technol.* **2020**, *121*, 105826. [CrossRef]
22. Zheng, D.; Hu, X.; Lin, Y.-S.; Chen, C.-H. Tunable multi-resonance of terahertz metamaterial using split-disk resonators. *AIP Adv.* **2020**, *10*, 025108. [CrossRef]
23. Ou, H.; Lu, F.; Liao, Y.; Zhu, F.; Lin, Y.-S. Tunable terahertz metamaterial for high-efficiency switch application. *Results Phys.* **2020**, *16*, 102897. [CrossRef]
24. Liang, Z.; Wen, Y.; Zhang, Z.; Liang, Z.; Xu, Z.; Lin, Y.-S. Plasmonic metamaterial using metal-insulator-metal nanogratings for high-sensitive refraction index sensor. *Results Phys.* **2019**, *15*, 102602. [CrossRef]
25. Xu, Z.; Lin, Z.; Cheng, S.; Lin, Y.-S. Reconfigurable and tunable terahertz wrench-shape metamaterial performing programmable characteristic. *Opt. Lett.* **2019**, *44*, 3944–3947. [CrossRef]
26. Xu, R.; Lin, Y.-S. Characterizations of reconfigurable infrared metamaterial absorbers. *Opt. Lett.* **2018**, *43*, 4783–4786. [CrossRef]
27. Pereira, M.J.; Matta, M.; Hirsch, L.; Dufour, I.; Briseno, A.L.; Gali, S.M.; Olivier, Y.; Muccioli, L.; Crosby, A.; Ayela, C.; et al. Application of Rubrene Air-Gap Transistors as Sensitive MEMS Physical Sensors. *ACS Appl. Mater. Interfaces* **2018**, *10*, 41570–41577. [CrossRef]
28. Wen, Y.; Liang, Z.; Lin, Y.-S.; Chen, C.-H. Active modulation of polarization-sensitive infrared metamaterial. *Opt. Commun.* **2020**, *463*, 125489. [CrossRef]
29. Manjappa, M.; Pitchappa, P.; Wang, N.; Lee, C.; Singh, R. Active Control of Resonant Cloaking in a Terahertz MEMS Metamaterial. *Adv. Opt. Mater.* **2018**, *6*, 1800141. [CrossRef]
30. Cong, L.; Pitchappa, P.; Lee, C.; Singh, R. Active Phase Transition via Loss Engineering in a Terahertz MEMS Metamaterial. *Adv. Mater.* **2017**, *29*, 1700733. [CrossRef]
31. Liu, M.; Susli, M.; Silva, D.; Putrino, G.; Kala, H.; Fan, S.; Cole, M.; Faraone, L.; Wallace, V.P.; Padilla, W.J.; et al. Ultrathin tunable terahertz absorber based on MEMS-driven metamaterial. *Microsyst. Nanoeng.* **2017**, *3*, 17033. [CrossRef] [PubMed]
32. Cheng, Z.; Toshiyoshi, H. Design of CMOS-MEMS broadband infrared emitter arrays integrated with metamaterial absorbers based on CMOS back-end-of-line. *Micro Nano Lett.* **2016**, *11*, 602–605. [CrossRef]
33. Pitchappa, P.; Manjappa, M.; Ho, C.P.; Singh, R.; Singh, N.; Lee, C. Active Control of Electromagnetically Induced Transparency Analog in Terahertz MEMS Metamaterial. *Adv. Opt. Mater.* **2016**, *4*, 541–547. [CrossRef]
34. Luo, Y.; Kikuta, K.; Han, Z.; Takahashi, T.; Hirose, A.; Toshiyoshi, H. An Active Metamaterial Antenna with MEMS-modulated Scanning Radiation Beams. *IEEE Electron Device Lett.* **2016**, *37*, 920–923. [CrossRef]
35. Haynes, W.M. (Ed.) *CRC Handbook of Chemistry and Physics: A Ready-Reference Book of Chemical and Physical Data*, 97th ed.; CRC Press: Boca Raton, FL, USA, 2016.
36. Palik, E.D. *Handbook of Optical Constants of Solids*; Academic Press: London, UK, 1985.
37. Huang, Q.-A.; Lee, N.K.S. Analysis and design of polysilicon thermal flexure actuator. *J. Micromech. Microeng.* **1999**, *9*, 64–70. [CrossRef]